Bringing Uncertainty into Focus: 'Control Climate Lens' Clarifies the Inter-Model Spread in Global Warming Projections

Xiaoming Hu[1], Patrick C. Taylor[2], Ming Cai[3,*], Song Yang[1], Yi Deng[4], and Sergio Sejas[2]

[1]Department of Atmospheric Sciences, Sun Yat-sen University, Guangzhou, China

[2]NASA Langley Research Center, Climate Science Branch, Hampton, Virginia, USA

[3]Department of Earth, Ocean & Atmospheric Sciences, Florida State University, Tallahassee, Florida, USA

[4]School of Earth and Atmospheric Sciences, Georgia Institute of Technology, Atlanta, Georgia, USA

* To whom correspondence should be addressed. E-mail: mcai@fsu.edu

Since Chaney's report[1], the range of global warming projections in response to a doubling of CO_2—from 1.5C to 4.5C or greater[2–7]—remains largely unscathed by the onslaught of new scientific insights. Conventional thinking regards inter-model differences in climate feedbacks as the sole cause of the warming projection spread (WPS)[8–12]. Our findings shed new light on this issue indicating that climate feedbacks inherit diversity from the model control climate. Regulated by the control climate sea ice coverage via its melt potential[13-18], models with greater (lesser) sea ice coverage generally possess a colder (warmer) and drier (moister) climate, exhibit a stronger (weaker) ice-albedo feedback, and experience greater (weaker) warming. The water vapor feedback also inherits diversity from the control climate but in an opposite way: a colder (warmer) climate generally possesses a weaker (stronger) water vapor feedback, yielding a weaker (stronger) warming. These inherited traits compete to influence the warming response obscuring the correlation between the WPS and control climate diversity. We envision this new insight and enhanced 'control climate lens' allow us to refocus an old yet underexplored line of inquiry contributing to the ultimate crack in the WPS armor and convergence of the warming projections.

Why do different climate models, under the same anthropogenic forcing, produce different amounts of global mean surface warming? A definitive answer to this question is central to the current scientific and societal deliberation, and will alter ongoing adaptation and mitigation efforts and future climate policy[2,3,19,20]. Efforts to address this question often focus on the climate model response and feedbacks[11,21,22], as a clear mathematical framework based on energy balance describes the relationship between climate feedbacks and surface warming. This 'climate feedback lens' has zoomed in on cloud feedback and revealed specifically marine stratocumulus low clouds[23,24] as the largest contributor to climate change uncertainty[25].This conventional view holds radiative feedbacks as the sole culprit for the global warming projection spread (WPS) while directing little attention to the diversity among model control climates (i.e. "control climate lens"). Although true in the mathematical sense, the view provided by the 'climate feedback lens' is incomplete obscuring the root causes of the WPS[22]. We argue here, as a few other have[26,27], that the WPS inherits characteristics from the diversity of model control climate states and this recognition provides a new pathway for understanding and reducing model uncertainty.

The foundation for the argument of 'control climate lens' is that a model's control climate must shape its future climate projection. Previous research provides an illustration of such 'inheritance', as the control climate sea ice characteristics regulate the ice-albedo feedback[13-18]. More extensive sea ice coverage contributes to a stronger ice-albedo feedback due to an increased potential for ice melt[12,16,17]. Therefore, the control climate influences a model's response to a radiative forcing by modulating the ice-albedo feedback strength. Stemming from its influence on climate feedbacks, the 'control climate lens' thus provides a more comprehensive view of WPS. The general applicability of 'control climate lens' requires

55 substantial diversities in the control climate state among models, and key variables
56 characterizing model control climate (including temperature, clouds, water vapor, and sea ice
57 etc.). Sizable inter-model spread exists across most control climate variables in CMIP5
58 models[28,29] and specifically in global mean surface temperature even before an anthropogenic
59 forcing is imposed (Supplementary Figure S1).

60 Why under the same solar forcing and atmospheric greenhouse gases do climate models
61 produce different control climates? Similar to the opening question the answer to both is that the
62 same underlying physical process parameterizations and embedded assumptions control model's
63 behavior, climate characteristics, and response[30,31]. Different approaches for handling unresolved
64 and poorly constrained physical processes alter model evolution and lead to different variable
65 combinations satisfying energy balance requirements. The possible existence of multiple
66 equilibrium climate states given the same external forcing provides an additional mechanism for
67 diversity[32,33]. The existence of multiple equilibrium climate states also ties to the fundamental
68 physical processes. Because the collective effects of various physical processes determine the
69 control climate state and climate response, forced climate simulations initialized from different
70 control climate states must inherit a portion of this diversity. Such diversity in the control
71 climates, under the same external forcing, does explain a portion of the uncertainty in global
72 warming projections, the subject of this study.

73 We consider 31 140-year CMIP5 (the phase 5 of the Coupled Model Intercomparison
74 Project) climate simulations under the same solar energy input plus a steady, 1% per yearCO_2
75 increase starting from the pre-industrial CO_2 concentration level of 280 PPMV (the 1pctCO2
76 experiments, Supplementary Table S1). We consider eight key climate variables (Supplementary
77 Table S2 and S3): (i) surface temperature (T), (ii) vertically integrated atmospheric water vapor

content (q), (iii) vertically integrated cloud water/ice content (CL), (iv) area covered by ice/snow (IC), (v) net downward radiative fluxes at TOA whose spatial pattern measures the strength of the total atmosphere-ocean energy transport (DYN), (vi) evaporation (E), (vii) the difference between surface evaporation (E) and precipitation (E – P) whose spatial pattern measures the strength of atmospheric latent heat transport, and (viii) surface sensible heat flux (SH). Considered at the time of CO_2 quadrupling ($4\times CO_2$), the transient climate response (denoted as Δ) is defined as the difference between the perturbed and control climate states specified as the average over the last 10-year period minus the first 10-year period.

Figure 1 shows $<\Delta T>$ as a function of model integration time ("<>" denotes the global mean). The WPS among these 31 simulations emerges shortly after the simulation begins displaying a range of 2.5 °C to 5.2 °C at $4\times CO_2$. Indicated by Fig. 2a, a significant portion of this WPS is explained by the diversity in key control climate variables. The largest correlation, between $<T>$ and WPS (–0.52), implies colder models experience greater warming; a feature illustrated by the color-coded curves in Fig. 1. Often accompanying colder $<T>$, models with larger $<IC>$ have greater melt potential (Fig. 2a and Supplementary Fig. S2), which favors an enhanced ice-albedo feedback and thereby a stronger warming[12,16,17]. The spread in dynamic heat transport also positively correlates (0.47; Fig. 2a) with WPS indicating that models with stronger poleward heat transport experience greater warming. Though weaker in magnitude, $<E>$, $<E-P>$, and $<CL>$ also show statistically significant correlations.

Applying the 'climate feedback lens,' spreads of climate feedbacks describe a significant portion of the WPS. The correlation between WPS and $<\Delta IC>$ (–0.83; Fig. 2b) indicates that more ice melt relates to larger warming. Figure 2b also shows large correlations of

100 $<\Delta E>$(=$<\Delta P>$) (0.85) and $<\Delta q>$ (0.81) with WPS; models with larger increases in $<\Delta E>$, $<\Delta P>$
101 and $<\Delta q>$experience greater warming. Unlike Fig. 2a, Fig. 2b indicates no other statistically
102 significant correlations, including those between $<\Delta CL>$ and WPS. In contrast to prevailing
103 thought, the lack of an $<\Delta CL>$ imprints on WPS in this analysis likely results from using changes
104 in global cloud water content, not cloud radiative effects.

105 The correlations in Fig. 2a suggest that the WPS inherits diversity from the control climate,
106 although through its influence on climate feedbacks. Employing a series of successive regression
107 analyses (see Method), we link the WPS to differences in climate feedbacks and then analyze the
108 associations of feedback differences with control climate features. As indicated in Fig. 2b,
109 $<\Delta IC>$, $<\Delta E>$ (=$<\Delta P>$), and $<\Delta q>$ each exhibits a nearly identical high correlation with the WPS.
110 We choose $<\Delta IC>$ as the starting point of the successive analysis because its associated control
111 climate spread (Fig. 3) is most similar to that associated with the WPS (Supplementary Fig. S2),
112 compared to other two possible permutations (Supplementary Fig. S3 for $<\Delta E>$ and Fig. S4 for
113 $<\Delta q>$). Figure 3 (inner panel) demonstrates the interdependence of the climate response variables
114 indicating that 41% and 25%of the spreads in $<\Delta E>$ and $<\Delta q>$ relate to $<\Delta IC>$, respectively.
115 Together with the correlation information in Fig. 2b, the analysis indicates that a stronger
116 warming projection accompanies greater depletion of $<\Delta IC>$, and increased $<\Delta E>$ and $<\Delta q>$.

117 The magnitude of a model's $<\Delta IC>$ relates to robust control climate characteristics. Figure 3
118 appraises the relationship between the zonal mean profiles of the 8 control climate variables and
119 $<\Delta IC>$model spread (outer panels). Warmer, rainier, more moist, and greater melting at the time
120 of $4\times CO_2$ is associated with a control climate that is (a) much colder, particularly over the
121 Antarctic, (b) much drier in the tropics but more moist in the northern extratropics, (c) less global

cloudiness, (d) more ice/snow coverage, particularly in the Antarctic, (e) a stronger poleward energy and moisture transport, as indicated by positive values of the net radiative fluxes at the TOA in the tropics but negative values in the polar regions (Fig. 3e), and (f) less rainfall, particularly over the deep tropics. We term this control climate-WPS relationship "type-A." Subject to an anthropogenic radiative forcing, the "type-A" relationship predicts that a model with a colder (warmer) control climate state experiences larger (smaller) warming with a greater (lesser) melting of ice/snow, stronger (weaker) enhancement of rainfall and evaporation, and greater (smaller) increase in water vapor.

The residual fields obtained by removing relationships with $<\Delta IC>$attribute the remaining WPS largely to the residual spread of $<\Delta q>$, denoted as $<\Delta q>_{res}$ (Supplementary Fig. S5). Fig. 4. (inner panel) shows that $<\Delta q>_{res}$ accounts for 75%, 31%, and 21% of the total spreads of $<\Delta q>$, $<\Delta E>$, and $<\Delta T>$, indicating that the coupling between $<\Delta q>$and the other climate responses (Supplementary Table S4) remains discernable after removing the portion coupled with $<\Delta IC>$ (Supplementary Fig. S5). As the second variable chosen in the successive regression analysis, $<\Delta q>_{res}$ accounts for 75%, 31%, and 21% of the total spreads of $<\Delta q>$, $<\Delta E>$, and $<\Delta T>$, respectively (inner panels of Fig. 4). Changes in the poleward energy ($<\Delta|DYN|>$) and latent heat ($<\Delta|E–P|>$) transport possess particularly strong correlations with $<\Delta q>_{res}$ (Fig. 4 and Supplementary Fig. S5). The residual spread signals that models with a greater increase in atmospheric water vapor, strengthened poleward energy transport as well as latent heat transport, and increased global cloud coverage warm more.

Robust relationships link the residuals of the control climate spread to $<\Delta q>_{res}$ and the remaining WPS (outer panels Fig. 4). While there are similarities to their counterparts from Fig.

144 3, some stark differences exist. In opposition to "type-A", the residual control climate spread
145 indicates that a warmer control climate with less ice coverage is associated with a greater
146 increase in water vapor and larger warming. We term this control climate-WPS relation as "type-
147 B". The "type-A" relation accounts for the spread of $\langle \Delta IC \rangle$ and most of the WPS, while the
148 "type-B" relation accounts for most of the remaining portion of the WPS and variance in $\langle \Delta q \rangle$.

149 Considering control climate diversity, global mean surface temperature response, and climate
150 feedbacks, a story emerges connecting WPS and control climate characteristics. The spreads of
151 $\langle \Delta IC \rangle$ and $\langle \Delta q \rangle$ exhibit robust relationships with control climate characteristics, signaling
152 inherited diversity. A "type-A" relationship indicates that a stronger (weaker) ice-albedo
153 feedback corresponds to colder (warmer) control climate with more (less) ice coverage and
154 greater (lesser) warming. Subsequently, a "type-B" relationship indicates that a stronger
155 (weaker) water vapor feedback corresponds to a warmer (colder) control climate with less (more)
156 ice/snow coverage and more (less) warming. For the type-A control climate, the spread in ice-
157 albedo feedback strength drives the WPS, whereas the water vapor feedback spread drives the
158 WPS for type-B. If type-A explained all of the WPS, we would expect a large inter-model spread
159 for the ice-albedo feedback but a relatively small one for the water vapor feedback with the
160 warming projection inversely proportional to the control climate temperature. The converse is
161 true for the type-B with the warming projection proportional to the control climate temperature.
162 Therefore, these control climate-climate response relationships dictate a small chance of finding
163 a model with an abnormally strong ice-albedo *and* water vapor feedback relative to other models.

164 This control climate-climate response behavior also explains the weaker correlations between
165 the WPS and the control climate diversity as compared to the climate response. Obscuring the
166 'control climate lens', the opposing effects of control climate diversity on the ice-albedo and

water vapor feedbacks are likely responsible for the lack of investigation into of control climate-WPS relationships to understand uncertainty. This new insight revealing the competing influences of control climate on the ice-albedo and water vapor feedbacks adds crispness to the perspective through the 'control climate lens'.

Though incomplete, our results open a new chapter to the WPS story. Robust links between control climate, climate response, and the WPS provide supporting evidence for "emergent constraints" refining climate model projections[34]. Specifically related to control climate temperature and ice/snow cover in the Antarctic and the Southern Ocean supporting ongoing efforts to understand the physics governing this region[26,27]. Unraveling relationships between the control climate state and climate response shows promise for reducing climate change uncertainty. In contrast to the conventional 'climate feedback lens', the more complete 'control climate lens' has gone unexploited. Given the significant diversity among model control climates, this approach shows significant potential for narrowing the WPS. We do not challenge conventional thinking but enhance it by demonstrating that the inter-model spread in climate feedbacks inherits diversity from model control climates. In other words, the 'control climate lens' contributes to WPS by shaping climate feedbacks. New insights about the competing influences of the control climate on ice-albedo and water vapor feedbacks mark an important new wrinkle. The 'control climate lens' allows us to probe deeper into the physics driving our climate models and their response. Hopefully, these new insights reopen an old and underexplored line of inquiry enabling us to pierce the unscathed armor surrounding WPS.

Methods

Data

All data used in this study are derived from the monthly mean outputs of the CMIP5 1pctCO2 experiments. We only consider the first 140 years of simulation output fields. Supplementary Table S1 provides the model names and spatial resolutions of the 36 1pctCO2 experiments' outputs that are archived and freely accessible at http://pcmdi9.llnl.gov/. We consider 31 of these models because (a) two of them were made without continuous increase of CO_2 concentration after reaching the $2xCO_2$ and (b) three models did not have all the required output fields, such as 3D cloud fields.

Key climate state variables and definitions of various averages

Eight key climate state variables are constructed at their native grids from the output fields listed in Supplementary Table S2. Supplementary Table S3 provides the definitions of the 8 key climate state variables and their units. Because the native grids of different 1pctCO2 experiments have different spatial resolutions, we first calculate the zonal average of each key climate state variable at 18 10-latitude wide bands, $\{\phi_0, (\phi_0 + \pi/18)\}$ with $\phi_0 = -\pi/2, -4\pi/9, \cdots, 4\pi/9, \pi/2$, according to

$$F_j(n) = \frac{9}{\pi^2} \int_{\phi_0}^{\phi_0+\pi/18} \cos\phi \, d\phi \int_0^{2\pi} f_j(n) \, d\lambda \qquad (1)$$

where λ is longitude and $f_j(n)$ is one of the 8 key climate state variables (i.e., n = 1, …, 8) at their native grids of the j^{th} 1pctCO2 experiment with j = 1, 2, …, 31.

We define the first 10-year average of $F_j(n)$ as the climate mean state of the j^{th} 1pctCO2 experiment, denoted as $\overline{F_j(n)}$. The ensemble mean of $\overline{F_j(n)}$ averaged over the 31 experiments is referred to as the ensemble mean climate state and the departure of $\overline{F_j(n)}$ for each j from the ensemble mean state measures the climate mean state diversity (or spread) of the j^{th} 1pctCO2 experiment, denoted as $\overline{F_j(n)}'$. The difference between the 10-year average of $F_j(n)$ taken from

130 to 140 years and $\overline{F_j(n)}$ corresponds to the (transient) climate response of $F_j(n)$ at the time of $4\times CO_2$, denoted as $\Delta F_j(n)$. The ensemble mean of $\Delta F_j(n)$ averaged over the 31 experiments is referred to as the ensemble mean climate response and the departure of $\Delta F_j(n)$ for each j from the ensemble mean climate response measures the uncertainty (or spread) in projecting the change/trend in the variable *f* by the j[th] 1pctCO2 experiment, denoted as $\Delta F_j(n)'$. The global mean of $\Delta F_j(n)'$ is obtained by averaging $\Delta F_j(n)'$over the 18 10-latitude wide bands, denoted as $<\Delta F_j(n)'>$.

Analysis Procedures

All variance, correlation, and regression calculations are done for inter-model spreads (i.e., the corresponding calculations are done over j). The statistical significance of correlations is evaluated using the Student's t-test. In the remaining discussion, we especially use $n = 8$ for surface temperature *T* and the rest of n (n = 1, 2, … 7) for the other 7 variables. The following is the procedure for calculating the results shown in Figures 3-5.

(a) Identify $n_0 \neq 8$ such that the correlation between $<\Delta T_j'>$ and $<\Delta F_j(n_0)'>$ is maximum among all $<\Delta F_j(n \neq 8)'>$.

(b) Construct the residual spread of x_j, where x_j is one of the 152 spreads (8 for $<\Delta F_j(n)'>$and 8×18 for 8 $\overline{F_j(n)}'$ at the 18 latitude bands), according to,

$$x_j^{residual} = x_j - a(<\Delta F_j(n_0)'>, x_j)<\Delta F_j(n_0)'> \quad (2)$$

where $a(<\Delta F_j(n_0)'>, x_j)$ is the regression coefficient between $<\Delta F_j(n_0)'>$ and $x_j$and $a(<\Delta F_j(n_0)'>, x_j)<\Delta F_j(n_0)'>$is the part spread of $x_j$that can be explained by the spread of

231 $< \Delta F_j(n_0)' >$ with the percentage of the explained spread variance equaling the ratio of the

232 variance of $a(< \Delta F_j(n_0)' >, x_j) < \Delta F_j(n_0)' >$ to that of x_j.

233 (c) Replace $< \Delta T_j' >$ with $< \Delta T_j' >^{residual}$ and x_j with $x_j^{residual}$ and repeat the steps (a) - (b) until

234 none of $< \Delta F_j(n)' >^{residual}$ is statistically significantly correlated with $< \Delta T_j' >^{residual}$.

235 Note that $< \Delta F_j(n_0)' >^{residual} \equiv 0$ for all j since by definition, $a(x_j, x_j) = 1$. It follows that we

236 always end up with a distinct value of n_0 in the new round of the steps (a) - (b).

237 **Online Content** Source Data, model variables, definitions and extended data display items are

238 available in the online version of the paper, references unique to these sections appear only in the

239 online paper.

240 **Acknowledgements**

241 This research was in part supported by National Key Research Program of China

242 (2014CB953900), the National Natural Science Foundation of China (41375081),National

243 Science Foundation (AGS-1354834, AGS-1354402 and AGS-1445956),NASA Interdisciplinary

244 Studies Program grant NNH12ZDA001N-IDS. Data used in this study are archived and freely

245 accessible at http://pcmdi9.llnl.gov/.

246 **Author contributions**

247 M. Cai conceived the idea for the study. X-M Hu downloaded the data and performed most of

248 the calculations. P. Taylor and M. Cai were the main writers of the first draft of the manuscript

249 and all the authors discussed the results and contributed to the final version of the

250 manuscript.Correspondence and requests for materials should be addressed to M. Cai

251 (mcai@fsu.edu).

References

1. Academy, N. & Sciences, O. F. *Carbon Dioxide and Climate*. (National Academies Press, 1979). doi:10.17226/12181

2. Meehl, G. A. *et al.* 2007: Global Climate Projections. *Clim. Chang. 2007 Contrib. Work. Gr. I to Fourth Assess. Rep. Intergov. Panel Clim. Chang.* 747–846 (2007). doi:10.1080/07341510601092191

3. Flato, G. *et al.* Evaluation of Climate Models. *Clim. Chang. 2013 Phys. Sci. Basis. Contrib. Work. Gr. I to Fifth Assess. Rep. Intergov. Panel Clim. Chang.* 741–866 (2013). doi:10.1017/CBO9781107415324

4. Stainforth, D. A. *et al.* Uncertainty in predictions of the climate response to rising levels of greenhouse gases. *Nature* **433,** 403–406 (2005).

5. Roe, G. H. & Baker, M. B. Why Is Climate Sensitivity So Unpredictable? *Science* **318,** 629–632 (2007).

6. Knutti, R. & Sedláček, J. Robustness and uncertainties in the new CMIP5 climate model projections. *Nat. Clim. Chang.* **3,** 1–5 (2012).

7. Webster, M. *et al.* Uncertainty Analysis of Climate Change and Policy Response. *Clim. Change* **61,** 295–320 (2003).

8. Hansen, J. *et al.* Climate sensitivity: Analysis of feedback mechanisms. *Clim. Process. Clim. Sensit. (AGU Geophys. Monogr. Ser. 29)* **5,** 130–163 (1984).

9. Boer, G. J. & Yu, B. Climate sensitivity and climate state. *Clim. Dyn.* **21,** 167–176 (2003).

10. Bony, S. *et al.* How Well Do We Understand and Evaluate Climate Change Feedback Processes? *J. Clim.* **19,** 3445–3482 (2006).

11. Andrews, T., Gregory, J. M., Webb, M. J. & Taylor, K. E. Forcing, feedbacks and climate sensitivity in CMIP5 coupled atmosphere-ocean climate models. *Geophys. Res. Lett.* **39,** 1–7 (2012).

12. Wigley, T. M. *et al.* Interpretation of high projections for global-mean warming. *Science* **293,** 451–4 (2001).

13. Rind, D., Healy, R., Parkinson, C. & Martinson, D. The Role of Sea Ice in 2xCO2 Climate Model Sensitivity. Part I: The Total Influence of Sea Ice Thickness and Extent. *J. Clim.* **8,** 449–463 (1995).

14. Dommenget, D. Analysis of the model climate sensitivity spread forced by mean sea surface: Temperature biases. *J. Clim.* **25,** 7147–7162 (2012).

15. Ashfaq, M., Skinner, C. B. & Diffenbaugh, N. S. Influence of SST biases on future climate change projections. *Clim. Dyn.* **36,** 1303–1319 (2011).

16. Rind, D., Healy, R., Parkinson, C. & Martinson, D. The role of sea ice in 2xCO(2) climate model sensitivity .2. Hemispheric dependencies. *Geophys. Res. Lett.* **24,** 1491–1494 (1997).

17. Holland, M. M. & Bitz, C. M. Polar amplification of climate change in coupled models. *Clim. Dyn.* **21,** 221–232 (2003).

18. Caldeira, K. & Cvijanovic, I. Estimating the contribution of sea ice response to climate sensitivity in a climate model. *J. Clim.* **27,** 8597–8607 (2014).

19. Randall, D. A. & Wood, R. A. Climate models and their evaluation. *Clim. Chang. 2007 Phys. Sci. Basis* 590–662 (2007).

20. Collins, M. *et al.* Long-term Climate Change: Projections, Commitments and Irreversibility. *Clim. Chang. 2013 Phys. Sci. Basis. Contrib. Work. Gr. I to Fifth Assess. Rep. Intergov. Panel Clim. Chang.* 1029–1136 (2013). doi:10.1017/CBO9781107415324.024

21. Vial, J., Dufresne, J.-L. & Bony, S. On the interpretation of inter-model spread in CMIP5 climate sensitivity estimates. *Clim. Dyn.* **41,** 3339–3362 (2013).

22. Wetherald, R. T. & Manabe, S. Cloud Feedback Processes in a General Circulation Model. *J. Atmos. Sci.* **45,** 1397–1416 (1988).

23. Bony, S. & Dufresne, J. L. Marine boundary layer clouds at the heart of tropical cloud feedback uncertainties in climate models. *Geophys. Res. Lett.* **32,** 1–4 (2005).

24. Webb, M. J. *et al.* On the contribution of local feedback mechanisms to the range of climate sensitivity in two GCM ensembles. *Clim. Dyn.* **27,** 17–38 (2006).

25. Dufresne, J. L. & Bony, S. An assessment of the primary sources of spread of global warming estimates from coupled atmosphere-ocean models. *J. Clim.* **21,** 5135–5144 (2008).

26. Trenberth, K. E. & Fasullo, J. T. Simulation of present-day and twenty-first-century energy budgets of the southern oceans. *J. Clim.* **23,** 440–454 (2010).

27. Grise, K. M., Polvani, L. M. & Fasullo, J. T. Reexamining the relationship between climate sensitivity and the Southern Hemisphere radiation budget in CMIP models. *J. Clim.* **28,** 9298–9312 (2015).

28. Brierley, C. M. Ocean Model Uncertainty and Time-Dependent Climate Projections. *Department of Meteorology*, **Ph.D.** Thesis**,** (The University of Reading, 2006).

29. Forster, P. M. *et al.* Evaluating adjusted forcing and model spread for historical and future scenarios in the CMIP5 generation of climate models. *J. Geophys. Res. Atmos.* **118,** 1139–1150 (2013).

30. Yoshimori, M., Hargreaves, J. C., Annan, J. D., Yokohata, T. & Abe-Ouchi, A. Dependency of feedbacks on forcing and climate state in physics parameter ensembles. *J. Clim.* **24,** 6440–6455 (2011).

31. Pedersen, C. A. & Winther, J. G. Intercomparison and validation of snow albedo parameterization schemes in climate models. *Clim. Dyn.* **25,** 351–362 (2005).

32. Saravanan, R. & Williams, J. C. M. Multiple Equilibria, Natural Variability, and Climate Transitions in an Idealized Ocean-Atmosphere Model. *J. Clim.* **8,** 2296–2323 (1995).

33. Knutti, R. & Hegerl, G. C. The equilibrium sensitivity of the Earth's temperature to radiation changes. *Nat. Geosci.* **1,** 735–743 (2008).

34. Klein, S. A, & Hall A. Emergent constraints for cloud feedbacks. *Curr. Clim. Change Rep.* **1**, 276-287 (2015).

.

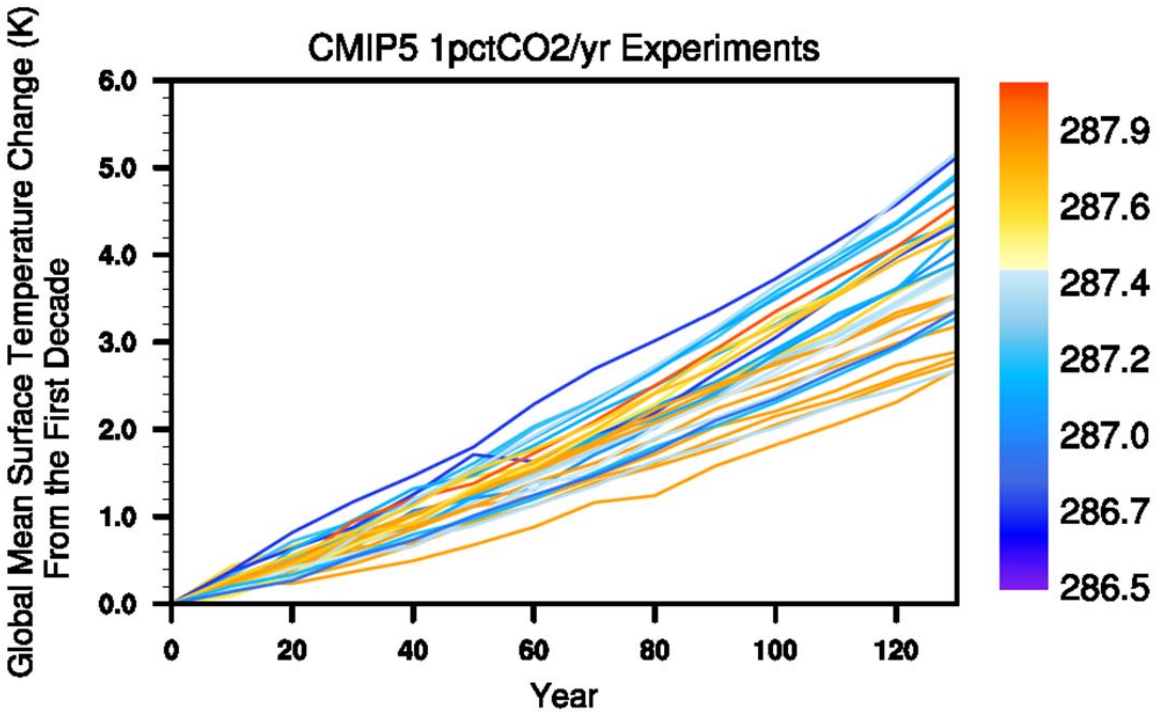

Figure 1Time series of global mean surface temperature change of the 31 CMIP5 1pctCO2 experiments relative to their corresponding first 10-year averages (labeled as "Year 0"). The color scheme for these 31 curves represents the global and time mean surface temperature of the first 10-year simulations of the 31 CMIP5 1pctCO2 experiments.

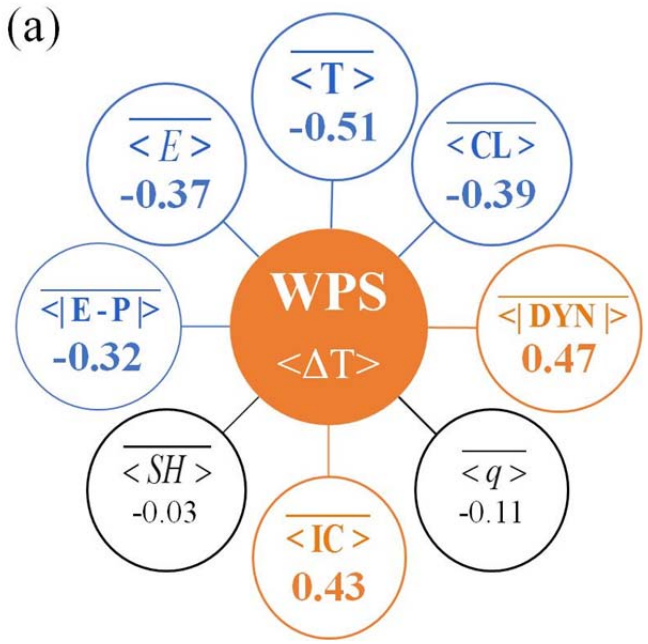

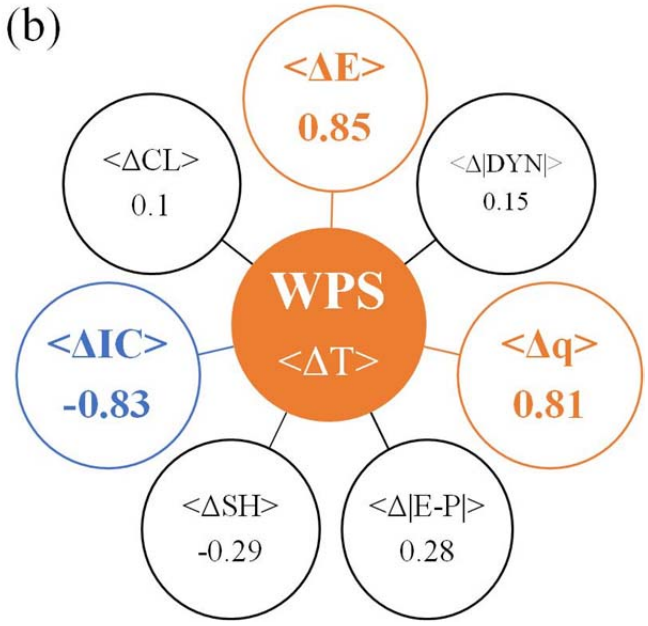

Figure 2. Correlation coefficients between the warming projection spread (WPS) and (a) spreads in the eight key control climate state variables, (b) spreads in the key climate variabletranseitnresponses to 4xCO_2. Colored numbers indicate the correlation coefficients exceed 90% confidence level.

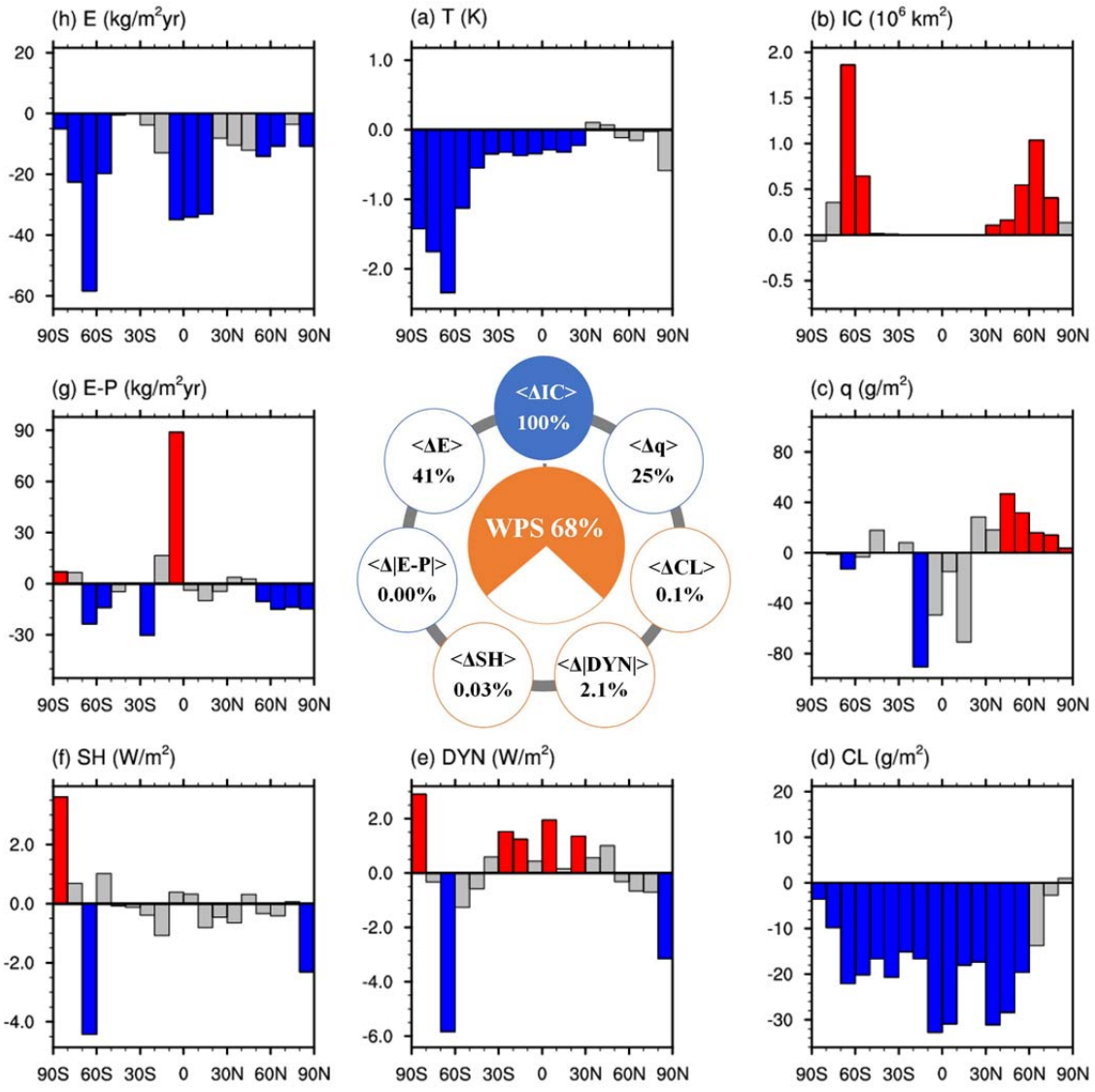

Figure 3. Latitudinal profiles (outer panels) of the regressed spreads of the zonal meancontrol climate states (a-h) against the projected spread in the change of total area coverage by ice/snow. (a) surface temperature (T in units of K), (b) total area covered by ice/snow (IC in units of km^2), (c) vertically integrated atmospheric water vapor content (q in units of g/m^2), (d) vertically integrated cloud water/ice content (CL in units of g/m^2), (e) net downward radiative fluxes at TOA which measures the strength of the total atmosphere-ocean energy transport (DYN in units of W/m^2), (f) surface sensible heat flux (SH in units of W/m^2), (g) difference between surface evaporation rate and precipitation rate ($E - P$ in units of kg/m^2/yr), and (h) precipitation rate (P in units of kg/m^2/yr). The numbers inside the circles of the inner panel correspond to the percentage of the spread, in the global mean changes of the eight key climate state variablesthat can be explained by the spread in the change of total ice/snow area coverage. Colored numbers/bars/circles indicate the correlation coefficients exceed 90% confidence level.

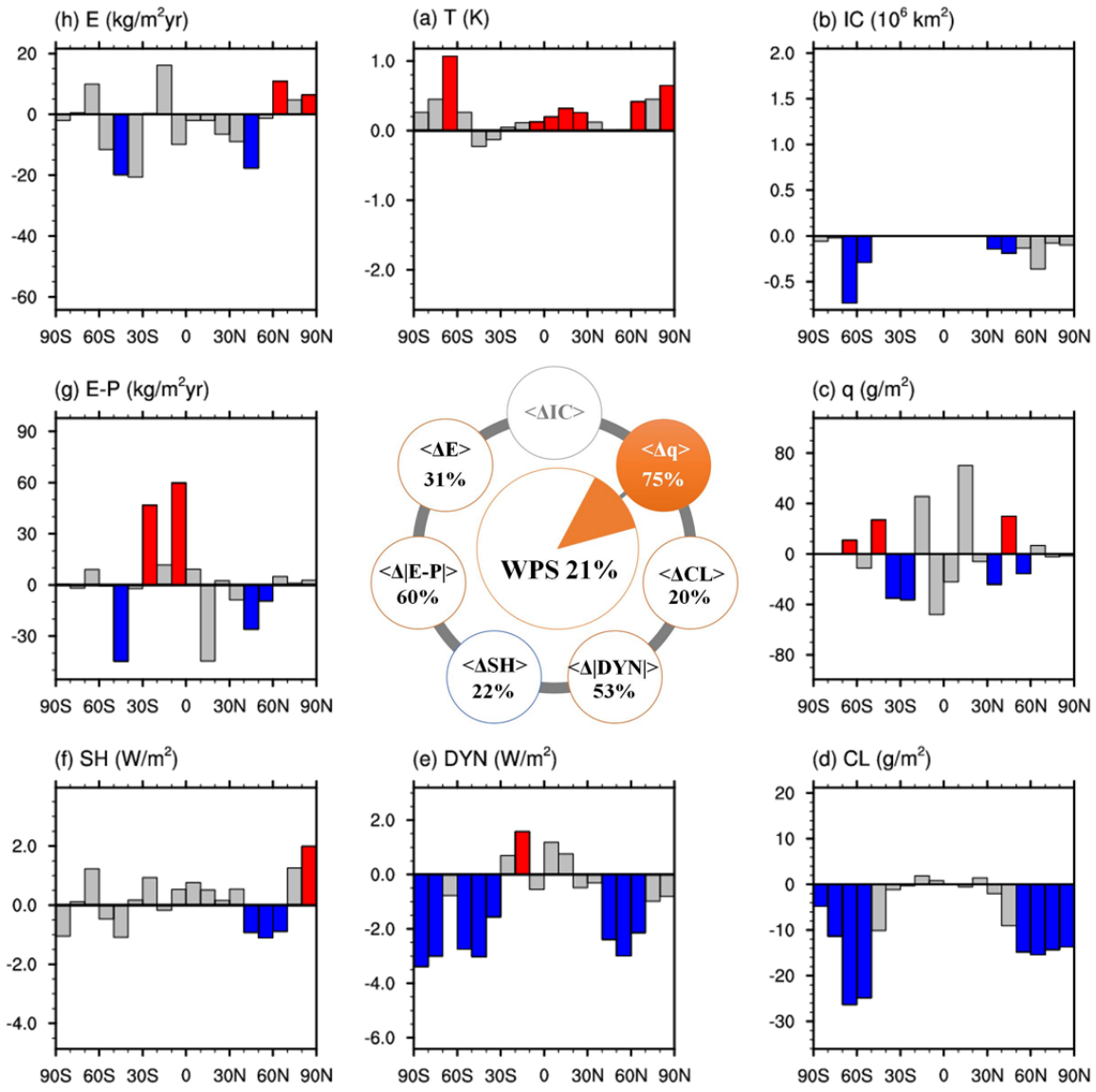

Figure 4. As in Figure 3 except for the portion of each corresponding variable not correlated with the spread the total ice/snow area coverage response. All correlations are made with the remaining spread (75%) in thetotal column-integrated atmospheric water vapor response. The numbers inside the inner panel circle still represent thepercentage of the spread, in the global mean changes of the eight key climate state variables, that can be explained by the remaining portion of the spread in thetotal column-integrated atmospheric water vapor response.